Methane Decomposition Over Modified Carbon Fibers as Effective Catalysts for Hydrogen Production

K. Sisáková[1] · A. Oriňak[1] · R. Oriňaková[1] · M. Strečková[2] · J. Patera[3] · A. Welle[4] · Z. Kostecká[5] · V. Girman[6]

Abstract

Catalyzed thermal decomposition of methane to produce hydrogen was studied. The carbon microfibers with embedded Ni, Cu and Co metals and metal phosphides were introduced as the novel catalysts. The catalysts were prepared by needle-less electrospinning being a versatile method for fibers production in large scale. The efficiency of methane decomposition by utilization of micro fiber carbon supported metal catalysts was studied by the pyrolysis-capillary gas chromatography method. The experiment was carried out in the temperature range from 973.15 to 1073.15 K. Kinetic parameters were calculated based on the Demitcheli kinetic model. It was found that the morphology, schedule of heat treatment and type and content of incorporated transition metals and metal phosphides may be the controlling parameter in the catalytic decomposition of methane. The highest conversion rates about 54% were achieved using carbon microfibers doped with cobalt and cobalt phosphide nanoparticles. The catalyst was heat treated in argon atmosphere followed by the hydrogen reduction. The second highest conversion rates were achieved with carbon microfibers doped with nickel and nickel phosphide nanoparticles carbonized only under argon atmosphere.

Graphic Abstract

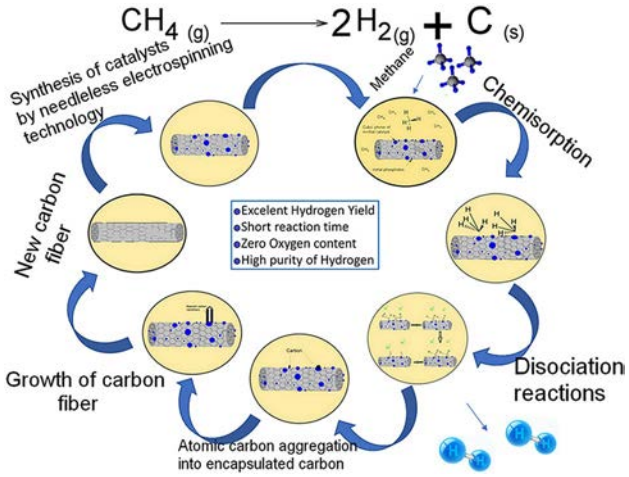

Keywords Pyrolysis · Catalysts · Methane · Hydrogen · Carbon microfibers

1 Introduction

The use of hydrogen in fuel cells is one of the most energy-efficient technologies of the twenty-first century. At present, annual hydrogen output is about 0.1 Gt per year. Most of

✉ A. Oriňak
andrej.orinak@upjs.sk

Extended author information available on the last page of the article

this hydrogen is obtained by steam reforming of fossil fuels, but it emits a huge amount of carbon dioxide, known as greenhouse gas. Annual hydrogen consumption is about 50 million tons of which 50% is for the NH_3 sector, 37% for oil refineries, 7% for CH_3OH and 6% for other areas [1]. Therefore, it is necessary to increase the production of hydrogen 100 times to meet the demand for fossil fuels. World statistics show that 48% of hydrogen is produced by steam reforming, 30% water electrolysis, 18% combustion of petroleum products, and 4% from coal [2, 3].

Thermal decomposition of methane (TDM) is one of the most promising and environmentally friendly methods for producing hydrogen, as no carbon oxides arise [4–6].

$$CH_4(g) \rightarrow C(s) + H_2(g)\Delta H_{298K} = 74.52kJ/mol \quad (1)$$

Due to the weak endothermic reaction of decomposition, the temperature around 873.15 K must be reached to achieve reasonable reaction rates. Therefore, the various metal and carbonaceous catalysts have been introduced in the interest of reducing decomposition temperature. Zhou et al. presented the efficiency of TDM using of 65 wt% Fe catalyst on alumina support and a bulk Ni catalyst, [6]. Catalyst efficiency was studied by TDM at 1023.15 K. In the case of Fe catalyst, the hydrogen yield was 780 mmol/g_{cat} and in the case of bulk Ni it was 450 mmol/g_{cat} [5, 7]. Reshetenko et al. prepared 90Fe–Al_2O_3, 85Fe–5Co–Al_2O_3 and 85Fe–5Ni–Al_2O_3 bimetallic catalysts [8]. TDM occurred at 898.15 K to carbon yields of 5.5 g/g_{cat}, 16 g/g_{cat} and 12.9 g/g_{cat}, respectively. The conversion of methane after 1 h for Fe–Al_2O_3, Fe–Co–Al_2O_3, and Fe–Ni–Al_2O_3 was 5.2%, 8% and 8.4%. Cansu Deniz et al. studied TDM by utilization of Fe–SiO_2 catalysts at 1073.15 K and thermal decomposition achieved a hydrogen yield of 2.3 mol/g_{cat} [9]. By introducing a Fe–Al_2O_3 catalyst a hydrogen yield of 0.6 mol/g_{cat} at 973.15 K was achieved [10]. A lot of similar catalysts were developed for effective hydrogen evolution via TDM by means of different catalyst with diverse morphology and structure: Ni catalyst with hydrogen yield of 66 mol/g_{cat} (773.15 K) [11], Ni (40 wt%)–SiO_2 reached a hydrogen yield of 32 mol/g_{cat} (773.15 K) [12], 2:1:1 trimetallic Ni–Fe–Al alloy, with a hydrogen yield of 92 mol/g_{cat} (923.15 K) [13]. TDM in a fluidized bed of carbon black particles can provide more than 40% hydrogen in longer time at optimum operating temperature of 1193.15–1213.15 K [14].

In the last decade, the carbon-catalyzed decomposition of methane like at nanostructured carbons, carbon nanotubes, fullerenes of graphene have been recognized as most attractive features for fuel cell [15]. Accordingly, a great deal was focused on methane decomposition over transition metal as a catalysts doped on carbon surface [16, 17]. However, the decrease of catalytic activity due to the deactivation of the catalysts surface by the formation of a carbon deposition caused technical problems due to a generation of contaminated hydrogen with carbon oxides (incoming from traces of molecular oxides after feedstock pyrolysis) requiring a further purification step of the obtained product mixture.

The present paper deals with the preparation of carbon fibers by needle-less electrospinning technology as a one of the most versatile methods for the preparation of nano—or micro- fibers [18, 19]. Electrospinning is a widely used technique for the electrostatic production of nanofibers, during which electric power is used to make polymer fibers with diameters ranging from 2 nm to several micrometers. This process is a major focus of attention because of its versatility and ability to continuously produce fibers on a scale of nanometers, which is difficult to achieve using other standard technologies. The basic principle of electrospinning is based on generating free charges on the surface of polymer solution by a high voltage potential (in 10 kV), which overcomes the solution's surface tension and produces a charged Tailor jet of conical shape [20]. In a typical setting one or more needles (spinnerets) are generally used to draw the fibers from a solution or melt. However, the production rate of the single spinneret is very low, which implies strong limitations for mass production [21]. On the other hand, the needle-less (NLES) or free liquid surface electrospinning can generate numerous jets from the solution surface enhancing the production rate even one or two orders of magnitude in comparison to the conventional method [22].

The main goal of present work was focused on the comparison of the efficiency of hydrogen production via TDM using of three types of carbon catalysts, which were modified by incorporation of metals: Ni, Co, Cu and transition metals phosphides (TMPs) Ni_xP_y, Co_xP_y, Cu_xP_y into the carbon fibrous matrix. The structure of the prepared modified carbon fibers was analyzed by XRD pattern and the morphology and distribution of nanoparticles was characterized by means of SEM and TEM. The catalytic conversion of methane at different temperatures was studied and the mechanism of thermal decomposition of methane to hydrogen over carbon microfiber catalyst was suggested.

2 Experimental Methods

2.1 Materials and Methods

The modified fibrous samples were designed for the electrocatalytic production of hydrogen evolution reaction [23]. PAN—Polyacrylonitrile (Aldrich, Mw = 150,000 g/mol, DMF - *N*,*N*-dimethylformamide (Acros Organic, 99.8%), nickel chloride hexahydrate $NiCl_2 \times 6H_2O$ (p.a. Aldrich), cobalt chloride hexahydrate $CoCl_2 \times 6H_2O$ (p.a. Aldrich) and copper chloride $CuCl_2$ (p.a. Aldrich) was used to preparation of the solutions for electrostatic spinning without further

purification. Phosphoric acid H_3PO_4 (Merck, 85%) was used as the source of phosphates and for increasing the conductivity of the electrostatic spinning solution. The molar ratio of $MCl_2.xH_2O$/DMF/PAN/H_3PO_4 was 3 g/30 ml/3 g/300 µl.

Methane 2.5 (Messer Tatragas, Slovakia) was used for thermal decomposition of methane with purity of ≥ 99.95%.

The phase composition and thermal decomposition of the samples were analyzed by XRD (PhilipsX' PertPro, CuKα radiation). To characterize the structure of prepared fibrous samples the following techniques were used: SEM/FIB (ZEISS AURIGA COMPACT), TEM (JEOL, 2100F) equipped with the EDX analysis. The characterization of catalysts after TDM was done by TEM and ToF–SIMS.

ToF–SIMS (Time-of-Flight Secondary Ion Mass Spectrometry) was performed on a TOF.SIMS5 instrument (ION-TOF GmbH, Münster, Germany). This spectrometer is equipped with a bismuth cluster primary ion source and a reflectron type time-of-flight analyzer. UHV base pressure was $< 2 \times 10^{-8}$ mbar. For high lateral resolution the Bi source was operated in a non-bunched mode providing Bi^+ primary ion pulses at 25 keV energy, 30 ns pulse width, and a spot size of approx. 150 nm. The sample was mounted by pressing it firmly into a bed of conductive glue, PLANO spectro tabs. To further reduce charging effects during analysis, an electron flood gun providing electrons of 21 eV was applied, and the secondary ion reflectron tuned accordingly. Prior to imaging the sample was cleaned by a brief oxygen sputter cleaning, using 500 eV oxygen ions until metal signals stabilized. For image recording, the primary ion beam was rastered across a 50×50 µm^2 field of view on the sample, and 256×256 data points were recorded, 1000 scans.

2.2 Preparation of Catalysts

Firstly, the pure PAN solution, was prepared by mixing of PAN and DMF at 353.15 K for 2 h. After homogenization of the PAN solution, 3 g of metal chloride were added and stirred at 333.15 K until complete dissolution of the metal chloride. Final spinned solutions PAN/metal chloride/H_3PO_4 were prepared by addition of 300 µl H_3PO_4 and then stirring for 1 h at 363.15 K until complete homogenization was achieved. The catalysts were prepared by needleless electrospinning. Solutions were spinned by devices Nanospider™ NS Lab with ELMARCO needleless electrospinning technology. The applied voltage was 50 kV and the spin distance between the spinner and the collector electrodes was within the range 120–130 mm. The electrostatic spinning process was carried out at ambient temperature with relative humidity 60%. Carbon fibers were prepared by a heat treatment process in a sintered furnace controlled by temperature and atmosphere. The sintering process was performed either in an inert Ar atmosphere at 1473.15 K or under an argon atmosphere at 1473.15 K, followed by a hydrogenation reduction step at 1023.15 K.

2.3 Methane Decomposition Experiment

The method of separation gas chromatography (GC) was used to study the efficiency of catalysts for TDM. Pyrolysis of the individual components took place in the micro-pyrolysis unit—Shimadzu Pyr-4A, attached to a chromatographic system consisting of two gas chromatographs—Shimadzu GC-17A.The pyrolysis reactor was made from quartz glass with length 18 cm and a width 3 mm. The reactor filler formed silicon carbide pellets to provide a piston flow of the reaction mixture and to minimize temperature fluctuations upon injection of the sample. During the single pyrolysis analysis, the chromatographic analytical system involved four elution channels with switching valves and two independent temperature programs. The residence time in the reaction zone was 0.356 s. Connecting chromatographs directly to the pyrolysis unit gives a relatively high reliability of evaluation of all pyrolysis products with a relative variation of 1–4%. Column C3 is chromatographic column Chrompack/PLOT CP–Al_2O_3/Kcl with length 50 m, internal diameter 0.32 mm and thickness of the film 5 µm was used.

Before each measurement, the instrument was calibrated using hydrogen, methane and mixtures as reference values. Calibration curves were plotted. From the directives of these linear dependencies, the amount of methane at the column outlet was calculated. The nitrogen phase was used as the mobile phase and the flow rate was set to 65 ml/min. The pressure at which the pyrolysis was carried out was constant and its value was 300 kPa. The pyrolysis temperature was measured in a temperature range of 1073.15–973.15 K. As was mentioned in the measurement, quartz reactors were used. The weight of the catalyst ranged from 2.5 to 3 mg. To the center of the quartz reactor we put a tweezer with a steel mesh. To achieve higher conductivity, carborundum was loaded onto this net. Catalyst of 2.5 mg load was added and carborundum was added to its surface in the same amount as before. After placing the reactor in the pyrolyzer, it was necessary to wait 5 min to stabilize and optionally purify the sample. The volume of methane was 0.2 ml.

3 Results and Discussion

3.1 XRD Characterization of Prepared Catalysts

Transition metal phosphides TMPs are known as capable of effectively promoting of hydrogen by TDM. The crystallinity of embedded metals and TMPs nanoparticles in the amorphous carbon matrix was observed by XRD patterns (Fig. 1). The presence of large amounts of

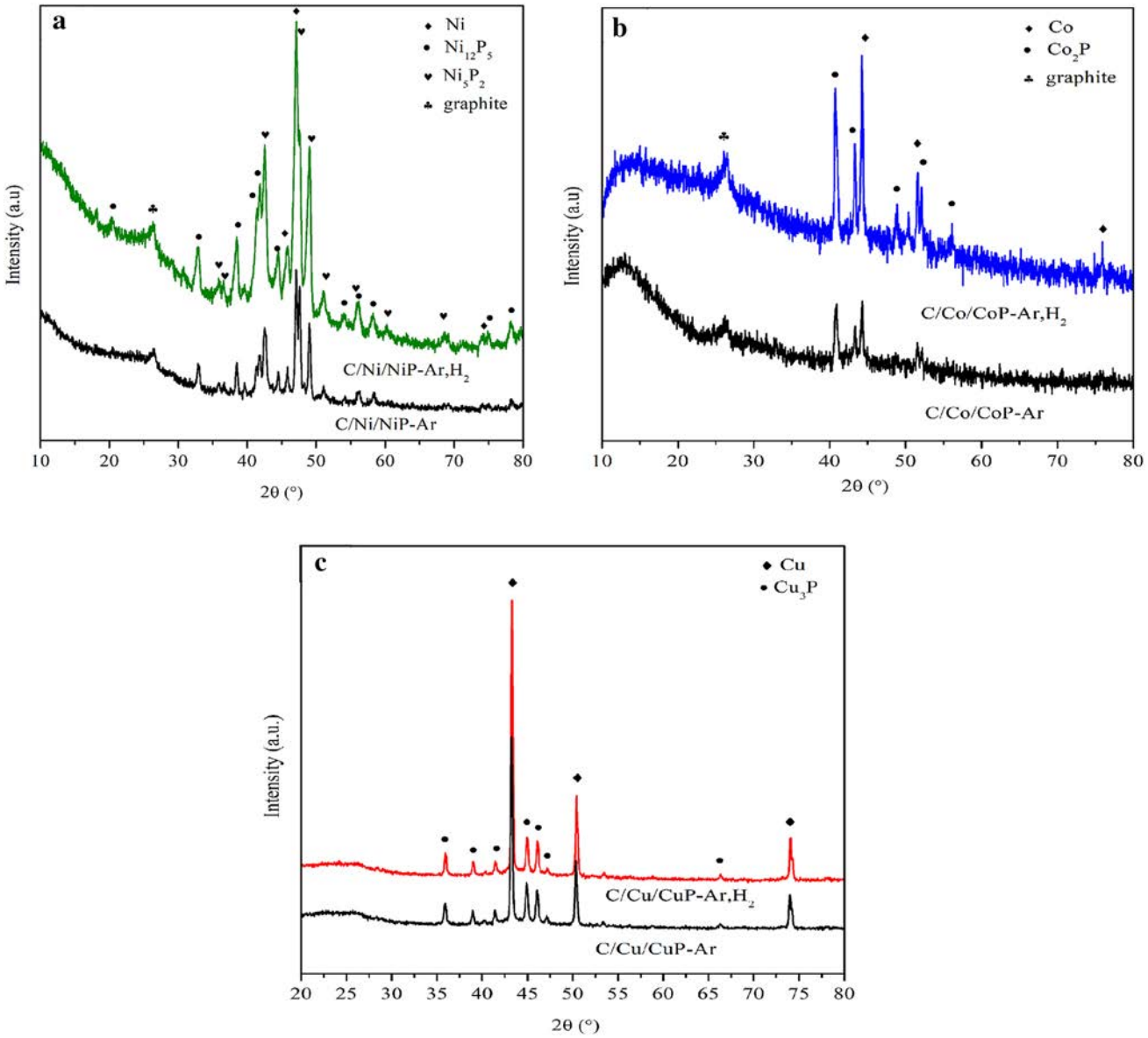

Fig. 1 XRD pattern of carbon modified catalysts carbonized in Ar or Ar/H_2 atmospheres **a** C/Ni/NiP, **b** C/Co/CoP, **c** C/Cu/CuP

amorphous carbon nanomaterials was indicated by two broad Bragg diffraction peaks (2Θ = 23.79° and 43.28°) in each XRD pattern of the prepared sample (mainly visible in the cases of C/Co/CoP, C/Cu/CuP). For all three samples, except of amorphous carbon the same metals and metals phosphides were confirmed in Ar or Ar/H_2 atmospheres. A small difference was observed in higher crystallinity of the metals and phosphides nanoparticles in the fibers thermally treated in the hydrogen atmosphere. For the C/Ni/NiP fibers, the diffraction peaks imply the cubic Ni phase (2Θ = 45.3°, 74°, COD 96-153-4893) and two types of phosphides: $Ni_{12}P_5$ (2Θ = 20.4°, 32.9°, 38.4°, 41.3°, 41.8°, 44.58°, 54.1°, 56.1°, 58.2°, 68.6°, 74°, COD 96-153-7574) and Ni_5P_2 (2Θ = 35.8°, 36.5°, 42.5°, 47.5°, 49°, 51.5°, 56.1°, 61°, COD 96-153-8448) in both aforementioned atmospheres (Fig. 1a). In the case of C/Co/CoP fibers, the similar observations were recorded where the pure Co cubic phase (2Θ = 43.8°, 51.1°, 75.1°, COD 96-901-2930) and one type of phosphide Co_2P (2Θ = 40.8 Θ, 43.3°, 48.7°, 51.9°, 56°, COD 96-900-9203) were identified (Fig. 1b). A strong graphitic signal was observed in the diffraction patterns of the C/Ni/NiP and C/Co/CoP fibers (2Θ = 26.2 Θ, COD 96-101-1061) [24]. Metallic Cu (2Θ = 43.2°, 50.3°, 74.2°, COD 96-500-0217) and Cu_3P phosphide nanoparticles (2Θ = 35.8°, 38.9°, 41.4°, 44.8°, 46°,47.1°, 66.2°, COD 96-810-4254) were indented in the XRD pattern in the both using atmospheres (Fig. 1c).

3.2 Morphology of the Prepared Catalysts

Based on SEM images it is clearly obvious that the morphology, porosity and microstructure of the final fibrous catalysts were essentially depended on the type of incorporated metals and TMPs and type of carbonization atmosphere. The regular fibrous morphology with a fiber diameter about 1 μm was determined in all three cases of prepared samples (Figs. 2a, 3a, 4a). C/Ni/NiP fibers containing nickel and TMP nanoparticles were homogeneously distributed along the fibrous structure (Fig. 2b). The minimum porosity was observed in the case of using pure Ar atmosphere (Fig. 2b). The created nanoparticles were localized inside as well as outside of carbon fibers. On the other hand the utilization of combined Ar and H_2 atmospheres lead to the highly porous structures with predominantly incorporated nanoparticles within the carbon matrix (Fig. 2c). The mentioned observation was revealed also by TEM images (Fig. 2e, f). Moreover two different nanoparticle sizes were observed (50 nm and 200 nm in diameter). The EDX analysis confirmed the chemical composition of fibrous samples which indicated presents of metals and TMPs nanoparticles (Fig. 2d).

Figure 3 show SEM images of C/Co/CoP fibrous samples carbonized in Ar and in the combined atmospheres of Ar and H_2. The carbonization of precursor's fibers in pure Ar atmosphere at 1473.15 K leaded to the creation of many angular agglomerates of phosphide nanoparticles on carbon matrix surface (Fig. 3b) with smooth surface morphology and minimal porosity of the fibers. A completely different morphology was observed when using a hydrogen atmosphere (Fig. 3c). SEM and TEM images revealed incorporation of nanoparticles into the carbon matrix and creation of curly nanoporous structure which apparently arise as a result of the formation of thick graphene layers (in some cases more than 50 nm thick) growing on a surface of cobalt or cobalt phosphide nanoparticles Fig. (3f). The reason for the creation of such an unusual structure is the introduction of the hydrogen environment at high temperature, which led to the entering of all external particles (formed on the surface) into the carbon thereby disrupting the compact carbon structure and causing the emergence of pores (Fig. 3e). The phosphide nanoparticles are efficient metal catalysts for hydrogen dissociation followed by hydrogen spillover. The spillover of hydrogen depends on the dissociative chemisorption of hydrogen on the transition or noble metal nanoparticles, and subsequent migration of hydrogen atoms on the adjacent surface by surface diffusion [25].

The morphology of the prepared copper-doped fibers C/Cu/CuP is complies with the low melting temperature of the copper (melting point of Cu is 1358.15 K). The melting and leaching out of the copper from carbon fibrous matrix at 1473.15 K in Ar atmosphere as a large spherical particles of copper with diameter of about 4 μm were observed in the Fig. 4a, b. These large copper agglomerates were predominantly located outside the fibers. After use of the reducing hydrogen atmosphere, incorporation of the nanoparticles

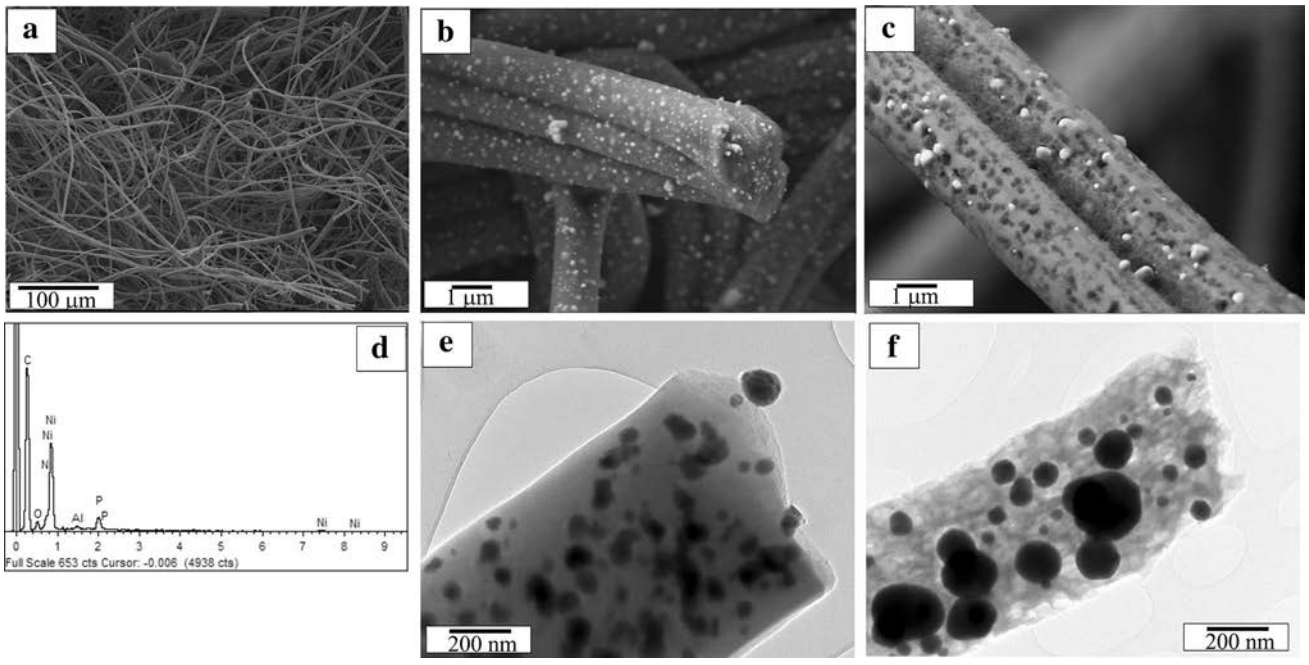

Fig. 2 Images of C/Ni/NiP sample: **a** fibrous morphology observed by SEM, **b** microstructure of one fiber heat treated in Ar atmosphere, **c** microstructure of one fiber heat treated in Ar/H_2 atmosphere, **d** EDX analysis of fiber heat treated in Ar/H_2 atmosphere, **e** TEM observation of fiber heat treated in Ar atmosphere, **f** TEM observation of fiber heat treated in Ar/H_2 atmosphere

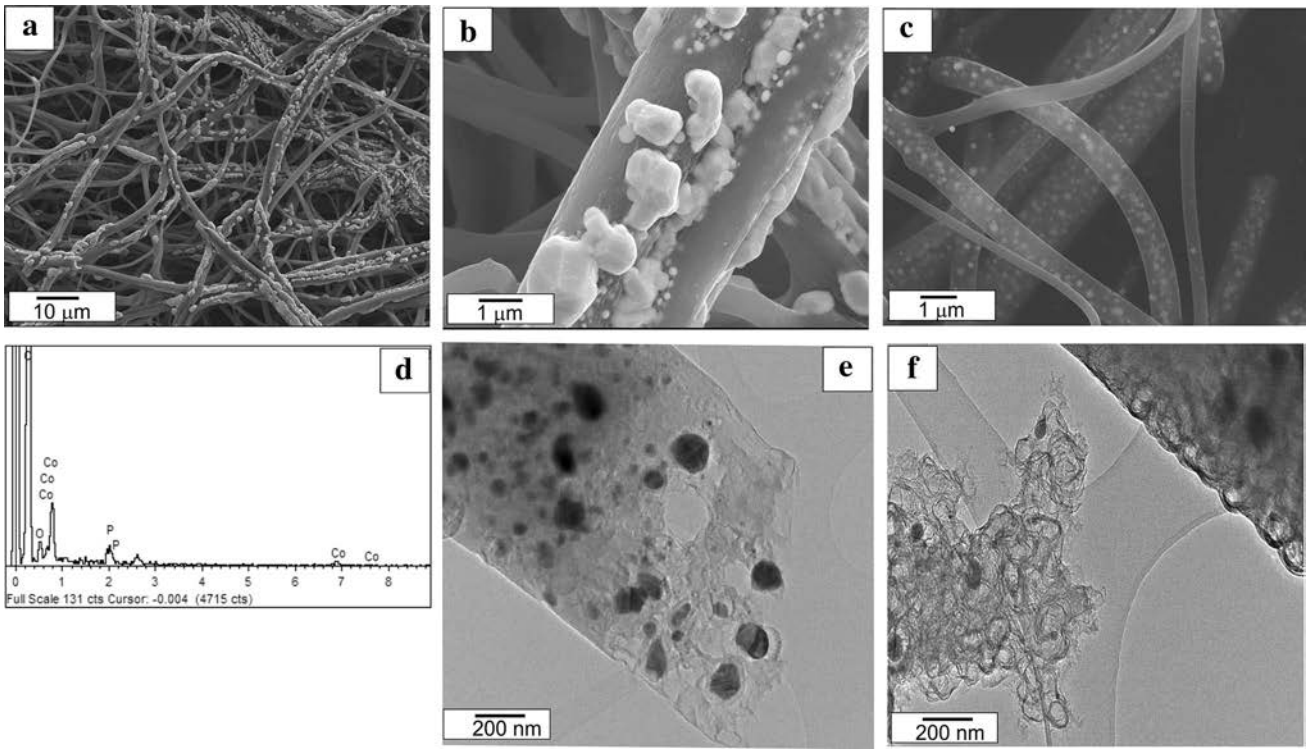

Fig. 3 Images of C/Co/CoP sample: **a** fibrous morphology observed by SEM, **b** microstructure of one fiber heat treated in Ar atmosphere, **c** microstructure of one fiber heat treated in Ar/H_2 atmosphere, **d** EDX analysis of fiber heat treated in Ar/H_2 atmosphere, **e** TEM observation of fiber heat treated in Ar atmosphere, **f** TEM observation of fiber heat treated in Ar/H_2 atmosphere

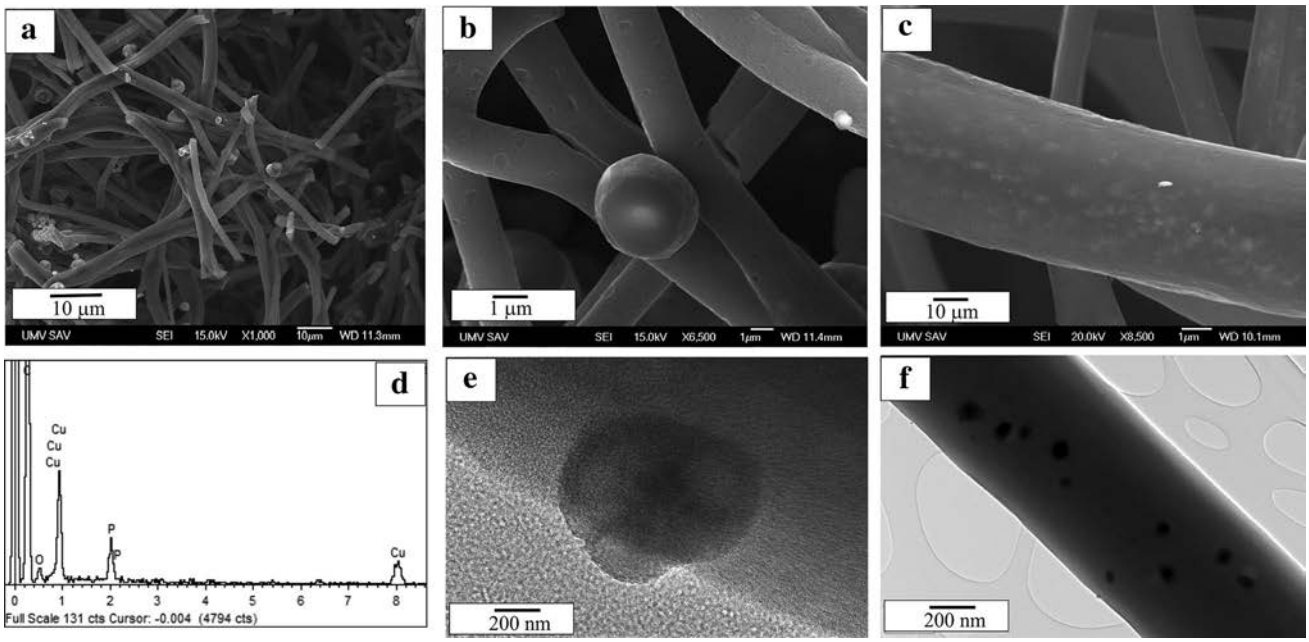

Fig. 4 Images of C/Cu/CuP sample: **a** fibrous morphology observed by SEM, **b** microstructure of one fiber heat treated in Ar atmosphere, **c** microstructure of one fiber heat treated in Ar/H_2 atmosphere, **d** EDX analysis of fiber heat treated in Ar/H_2 atmosphere, **e** TEM observation of fiber heat treated in Ar atmosphere, **f** TEM observation of fiber heat treated in Ar/H_2 atmosphere

into the internal fiber structure was observed (Fig. 4c, f). TEM images show small Cu_3P particles of 40 nm size homogeneously distributed in the fiber (Fig. 4f).

3.3 Catalytic Activity of Catalysts

Conversion of methane was calculated according to:

$$X = \frac{[CH_4]_{input} - [CH_4]_{output}}{[CH_4]_{input}} \times 100[\%] \quad (2)$$

where the CH_4 input value is the amount of methane at the inlet in milliliters and the value CH_4 is the amount of methane which was also in milliliters at the outlet. Yield of hydrogen was calculated based on:

$$Y_{H_2} = \frac{moles\ of\ hydrogen\ produced}{2 \times moles\ of\ CH_4 \in feed} \times 100[\%] \quad (3)$$

In pursuance of producing CO_2 free hydrogen, methane decomposition mechanism as given schematic in Fig. 5 mainly involves five steps as follows [15–18]:

1. The chemisorption of methane on the leading face of a catalyst particle

$$CH_4 + I\ (\text{vacant site}) \rightarrow CH_{4\,a} \quad (4)$$

where $0 < x < 2$; subscripts (a), (c) and (g) denote adsorbed, crystalline and gaseous species, respectively.

2. Detachment of a chemisorbed methane molecule through progressive breaking of four C–H bonds as follows:

$$(CH_4)_g \rightarrow (CH_3)_a + (H)_a \quad (5)$$

This step is followed by a series of surface stepwise dissociation reactions leading to elemental carbon and hydrogen

$$(CH_{3-x})_a \rightarrow (CH_{2-x})_a + (H)_a. \quad (6)$$

2. Aggregation of adsorbed atomic hydrogen into molecules, followed by gas phase emission

$$2(H)_a \rightarrow (H_2)_g \quad (7)$$

4. Atomic carbon aggregation into encapsulated carbon, leading to progressive catalyst deactivation, or atomic carbon diffusion through the bulk catalyst from the leading face to the trailing face, driven by the strong concentration gradient.
5. Carbon nucleation followed by the formation and growth of carbon nano-fibers (CNFs) in the trailing face of the catalyst particle.

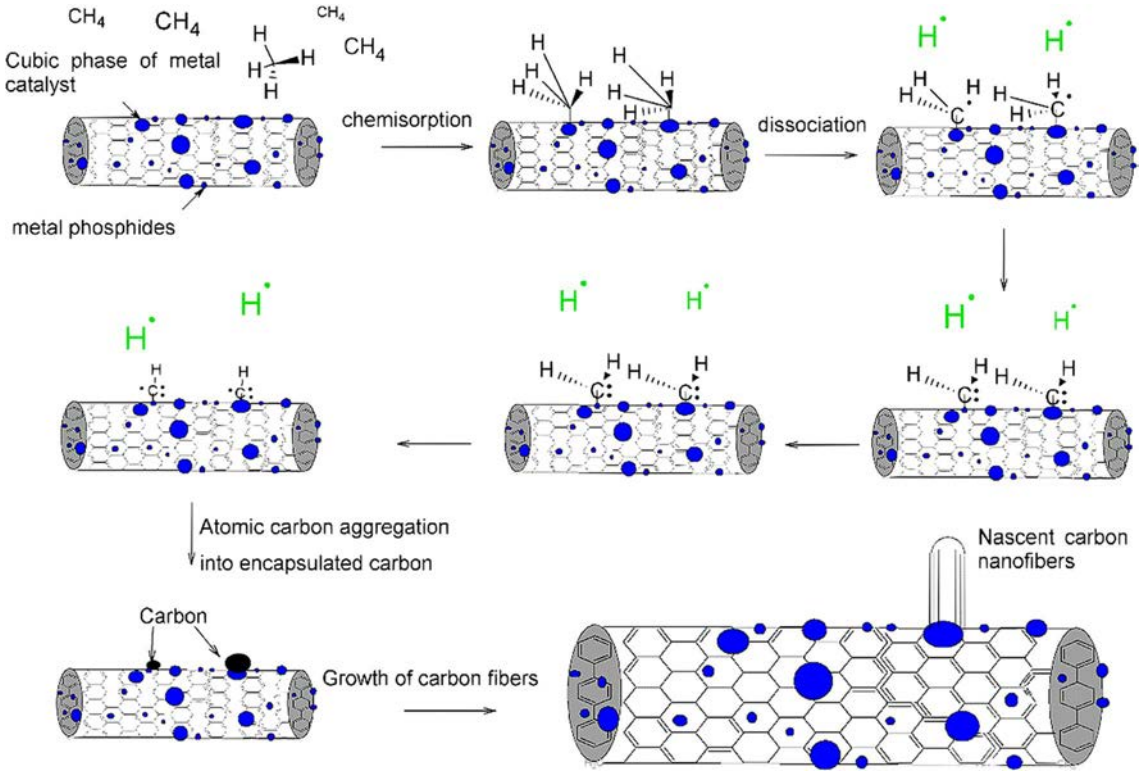

Fig. 5 Scheme of mechanism of thermal decomposition of methane to hydrogen over carbon microfiber catalyst doped with metals

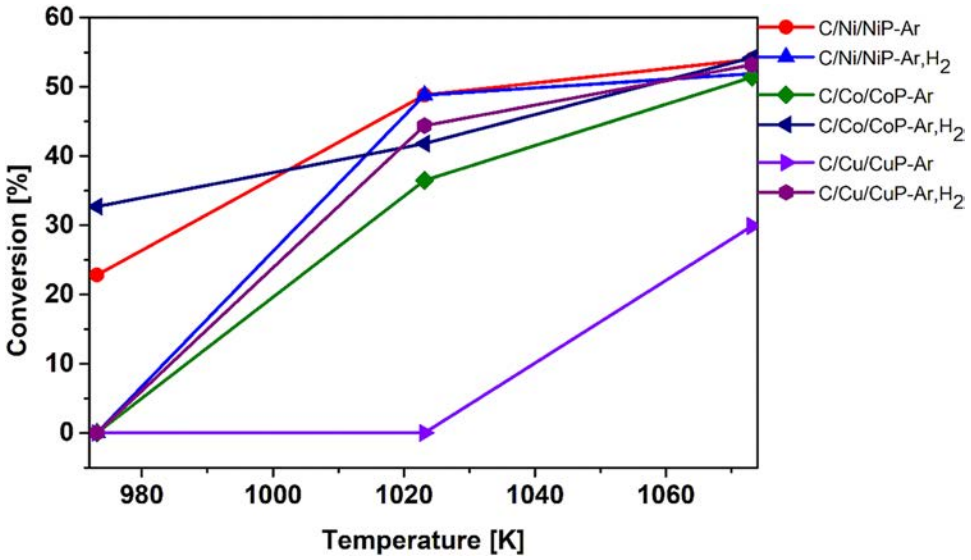

Fig. 6 Relationship of catalytic conversion of methane at different temperatures

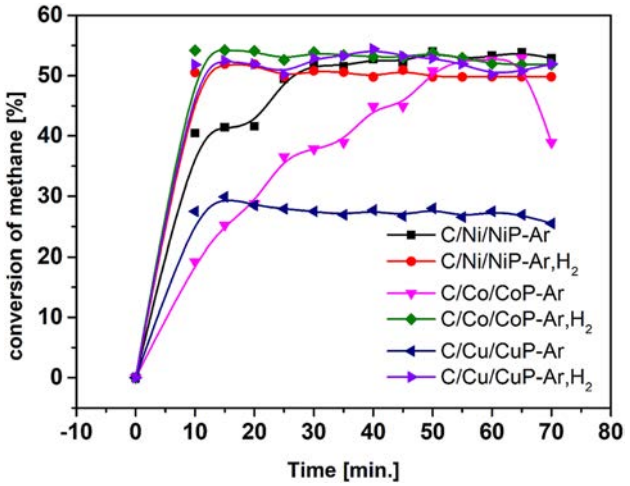

Fig. 7 Time relationship on methane conversion

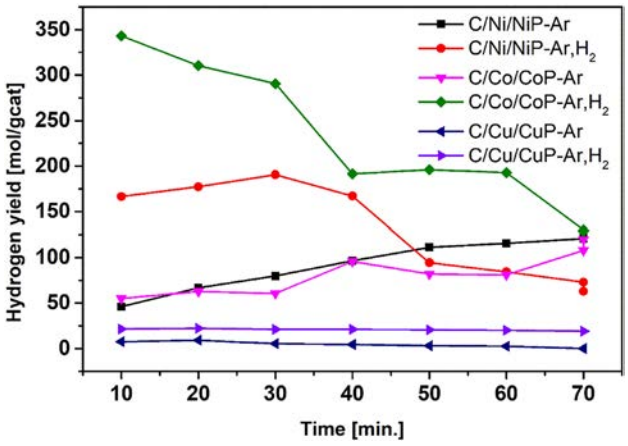

Fig. 8 Hydrogen yield with time at 1073.15 K temperature and pressure 300 kPa

Carbon crystalline growth:

$$(C)_a \rightarrow 1/n\ \left(C_n\right)_C \tag{8}$$

Figure 6 presents the dependence of conversion of methane on temperature. It has been observed that the catalysts which have been sintered in addition to the argon atmosphere even in the hydrogen atmosphere have a higher percentage of methane conversion and better efficiency even at lower temperatures. Thermal decomposition of methane occurred at temperatures of 973.15 to 1073.15 K, with conversion of about 30% for C/Ni/NiP-Ar, C/Co/CoP–Ar,H_2. The highest conversion rate of −54.4% was achieved using a C/Ni/NiP–Ar catalyst containing the highest metal content of 23.8 wt% and using a C/Co/CoP–Ar,H_2 catalyst of −54.2% with a metal content of 21.2 wt%. Figure 7 shows the stability of the catalysts at 1073.15 K and 300 kPa. The same amount of methane was added to the sample every 10 min. It is observed that catalysts which have been sintered in the hydrogen atmosphere are stable and their activity is about 50% even after 1.5 h. However, catalysts which have been sintered only under an inert argon atmosphere initially have a lower activity which increases with time to a certain value and then gradually decreases. This is because the hydrogen generated in the reactor forms a reducing hydrogen atmosphere which enhance the incorporation of phosphides into the carbon microfibre and thereby improve their activity. Also due to the hydrogen atmosphere the porosity of fibers increase. Figure 8 shows the yield of hydrogen over time. Although, the highest percentage of conversion had a C/Ni/NiP–Ar catalyst the highest amount of hydrogen yield was with the C/Co/CoP–Ar,H_2 catalyst. The results are comparable to the literature. Yield of hydrogen rises with temperature but

with growing yield time decreases. The reason is the high reaction rate of carbon deposition at a given temperature. Carbon is excreted on the catalyst surface and thus reduces its activity. Also, at higher temperatures the catalyst loses its morphology due to sintering [4, 26].As can be seen from Fig. 9, the highest maximum deposition rate of carbon has a C/Cu/CuP–Ar catalyst which also has the lowest conversion rate. Conversely, the lowest rate of carbon deposition has a C/Co/CoP–Ar,H_2 catalyst, which also has the highest conversion rate. The rate

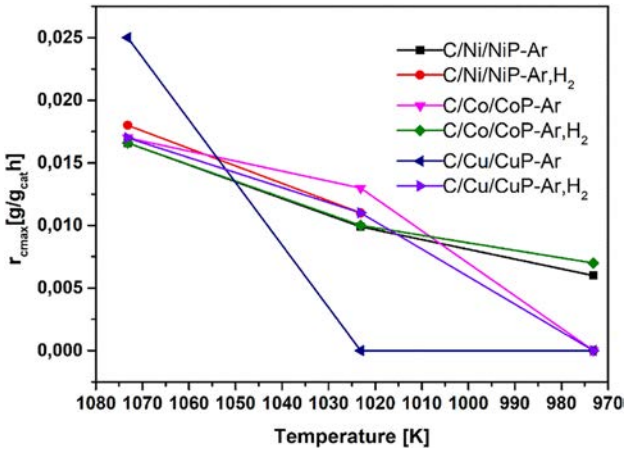

Fig. 9 Relationship of the maximal carbon deposition rate rcmax versus temperature

of carbon deposition as well as the conversion of methane with the temperature decrease. Yield of hydrogen, weight of hydrogen prepared per 1 g of catalyst m, catalytic efficiency X_{CH4} and kinetic parameters–maximum carbon deposition rate r_{cmax}, activity and total velocity at time t r were calculated according to Demichelis kinetic model in Table 1. In this kinetic model [27, 28], a separable kinetic technique has been introduced to create the velocity equation. The authors used two dependent variables to calculate the speed. The first was the deposition rate of carbon without deactivation of r* and the second was the activity factor. The actual rate of deposition of carbon at any point r is equal to r* product and activity. The carbon deposition rate r* is defined as the maximum deposition rate of carbon at time t, where a is an activity coefficient corresponding to a reduction in the maximum deposition rate of carbon due to blockage of active sites. This model was able to accurately predict the rate and method of deactivation of the investigated catalyst [29, 30]. The rate determining step was Eq. 1. Based on methane adsorption, Demicheli et al. developed the following equation for calculating the maximum deposition rate of carbon and the activity of the catalyst:

$$r_{cmax} = \frac{k\left(p_{CH_4} - \frac{p_{H_2}}{K_p}\right)}{\left(1 + K_H p^{0.5} H_2\right)^n} \tag{9}$$

and for activity:

Table 1 Catalytic activity of various metallic catalysts, calculated maximal deposition rate of carbon $r_{c,\,max}$, activity and the total speed of reaction

Sample	Temperature (K)	Yield of H_2 (mol/g_{cat})	m (g/g_{cat})	X_{CH4} (%)	r_{cmax} (g/g_{cat} h)	a	r (g/g_{cat}h)	Metal content (wt%)
C/Ni/NiP–Ar	1073.15	98.53	0.0267	54.4	0.0166	0.99	0.0165	23.8
C/Ni/NiP–Ar,H_2	1073.15	190.48	0.0516	51.92	0.018	0.99	0.017	20.1
C/Co/CoP–Ar	1073.15	119.56	0.0324	51	0.017	0.99	0.0169	16.3
C/Co/CoP–Ar,H_2	1073.15	343.16	0.093	54.2	0.0166	0.99	0.0165	21.2
C/Cu/CuP–Ar	1073.15	9.2	0.002	29.9	0.025	0.97	0.025	18.7
C/Cu/CuP–Ar,H_2	1073.15	22.2	0.006	53.2	0.017	0.95	0.017	20.9
C/Ni/NiP–Ar	1023.15	65.4	0.0178	40.2	0.0099	0.996	0.0099	23.8
C/Ni/NiP–Ar,H_2	1023.15	72	0.02	48.8	0.011	0.99	0.01	20.1
C/Co/CoP–Ar	1023.15	69.41	0.0188	36.5	0.013	0.994	0.013	16.3
C/Co/CoP–Ar,H_2	1023.15	129.9	0.0352	41.8	0.01	0.999	0.01	21.2
C/Cu/CuP–Ar	1023.15	0	0	0	0	0	0	18.7
C/Cu/CuP–Ar,H_2	1023.15	21	0.0057	49	0.011	0.98	0.011	20.9
C/Ni/NiP–Ar	973.15	32.24	0.009	22.8	0.006	0.997	0.006	23.8
C/Ni/NiP–Ar,H_2	973.15	0	0	0	0	0	0	20.1
C/Co/CoP–Ar	973.15	0	0	0	0	0	0	16.3
C/Co/CoP–Ar,H_2	973.15	28.4	0.0077	32.7	0.007	0.997	0.007	21.2
C/Cu/CuP–Ar	973.15	0	0	0	0	0	0	18.7
C/Cu/CuP–Ar,H_2	973.15	0	0	0	0	0	0	20.9

The data were calculated by Demicheli‘s kinetic model

$$a = exp\left(\frac{-k_d p_{CH_4} \tau}{p_{H_2}}\right) \quad (10)$$

$\tau = t - t^*$

then the total speed at time t is:

$$r = r_{cmax} \times a \quad (11)$$

where k is the specific rate constant for the rate of carbon deposition (g/g_{cat} h kPa),Kp is the equilibrium constant for the decomposition of methane (kPa), K_H is the equilibrium hydrogen adsorption constant ($kPa^{-0.5}$), k_d is the specific velocity constant for velocity deactivation (h^{-1}), t* is the time at which the rate of methane deposition reaches a maximum (h) and n is the number of active sites participating at the rate determining step, most frequently n = 7 [31, 32].

The calculated maximum deposition rate of carbon and therefore the overall rate at time t is lower than that reported in the literature [22–25]. However, different experimental conditions, higher pressure, space velocities were used.

3.4 Morphology of the Catalyst After TDM

3.4.1 TEM Characterization

Three types of carbon were produce based on TEM images. In the case of C/Ni/CNiP catalyst we can see from Fig. 10a that nickel particle is covered with graphite layers. Presland and Walker have designed a mechanism in which graphite layers are formed on the metal surface due to surface diffusion of atomic carbon atoms [33]. However, only surface diffusion does not occur. Atomic carbon can diffuse along the surface of the metallic nanoparticle to the other side and form carbon fibers as shown in Fig. 10b [34–36]. In the case of C/Co/CCoP catalysts TEM images shows carbon plates produced on the carbon fiber (Fig. 11a, b). It can be concluded that the carbon plates has elliptical shape with size of 200 nm in diameter [37]. In the case of C/Cu/CCuP catalysts TEM images did not show carbon formation (Fig. 12a, b). This was due to the low catalyst activity.

3.4.2 TOF–SIMS Characterization

A used Ni catalyst was subjected to ToF–SIMS surface analysis. Since the mounting of this sample included an organic glue being a source of carbon contamination, the specimen was precleared in-vacuo by a brief oxygen sputter step until the metal signals stabilized. Another wanted effect of this oxygen bombardment is the implantation of some oxygen into the (metal) matrix, enhancing the yield of $metal^+$ ion formation in the SIMS process. Apart from nickel, some potassium and sodium was detected on the fiber, these alkali metals, however, were not colocalized with the nickel imaged in Fig. 13. From these measurement we can see individual Ni patches sitting on a fiber of approx. 8 µm diameter.

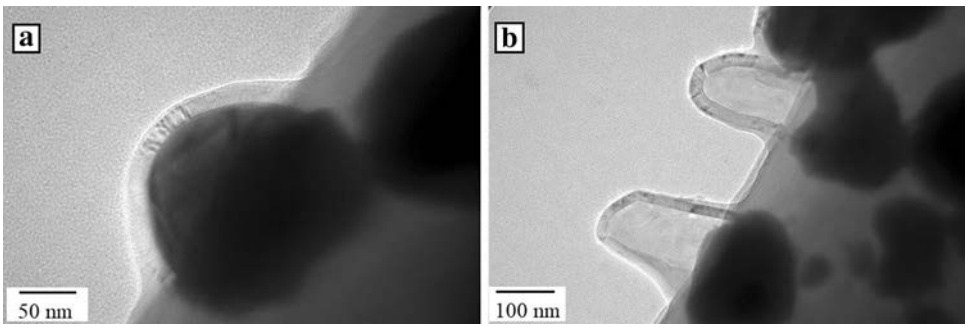

Fig. 10 Images of C/Ni/NiP sample after TDM

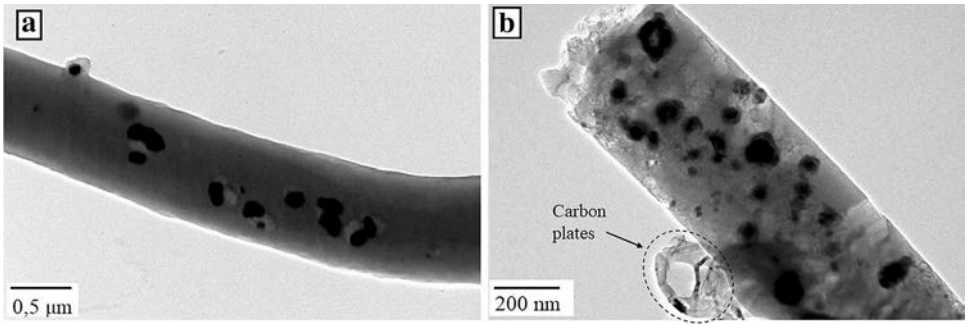

Fig. 11 Images of C/Co/CoP sample after TDM

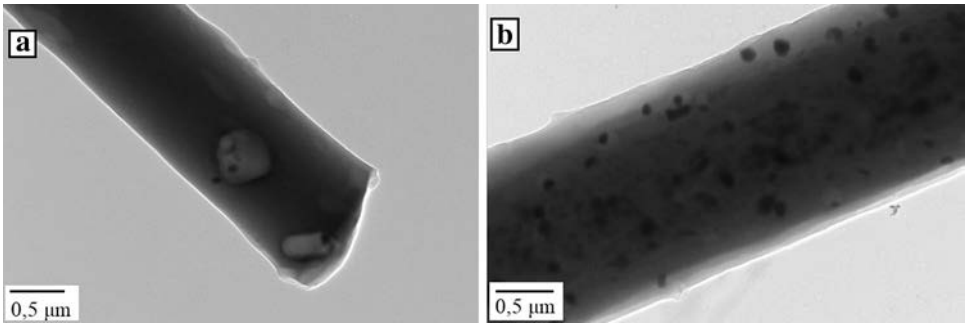

Fig. 12 Images of C/Cu/CuP sample after TDM

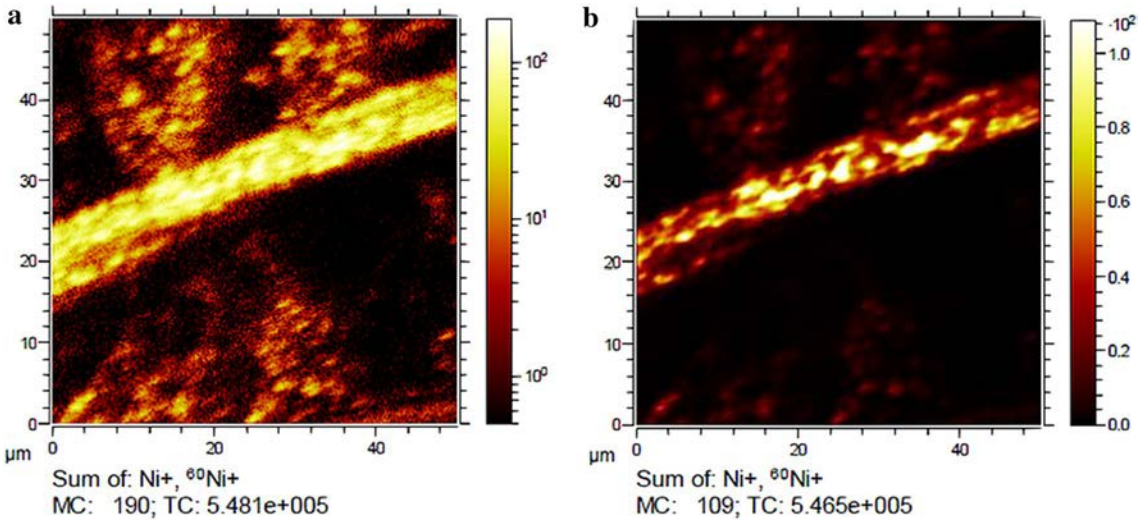

Fig. 13 SIMS characterization of C/Ni/NiP–Ar catalyst after TDM reaction. Sum of both nickel main isotopes, 58Ni and 60Ni. Image **a** with log. intensity scale, image **b** with linear intensity scale and 5-point averaging to improve the contrast in the Ni rich zones on the fiber

4 Summary

The catalytic efficiency of carbon microfibers doped with Ni, Co and Cu for thermal decomposition of methane produced hydrogen were studied and the kinetic parameters of conversion were determined. Catalysts were prepared by needle-less electrospinning; the first group was sintered only under an argon atmosphere and the other in addition to an inert argon atmosphere were also sintered in a reducing hydrogen atmosphere. Carbon microfiber was used as support for the catalyst. The most important advantage of this support is that it is oxygen-free, so there is no possibility of carbon monoxide side product formation. The conversion was studied at a temperature range of 1073.15–973.15 K, a pressure of 300 kPa and a flow rate of 65 ml/min. The highest percentage of conversion of methane to hydrogen was achieved using CNiP catalysts with the highest metal content 23.8 wt%. Catalysts that have been sintered only under the argon atmosphere have a low conversion rate, but with time conversion rate growing. This is due to the fact that the generated hydrogen produces a reducing atmosphere and thus affects the structure of the catalyst. Catalysts that were synthesized in the synthesis process even in the hydrogen atmosphere are, on the contrary, stable, with a higher conversion rate.

Acknowledgements This work was supported by the Scientific Grant Agency of the Ministry of Education, Science, Research, and Sport of the Slovak Republic Projects No. VEGA 1/0074/17, and Slovak Research and Development Agency under the Contract No. APVV 16-0029.

References

1. Colmati F, Alonso CG, Martins TD et al (2018) Production of hydrogen and their use in proton exchange membrane fuel cells. Adv Hydrog Gener Technol. https://doi.org/10.5772/intechopen.76663
2. Zhou L, Enakonda LR, Harb M et al (2017) Fe catalysts for methane decomposition to produce hydrogen and carbon nano materials. Appl Catal B 208:44–59. https://doi.org/10.1016/j.apcatb.2017.02.052

3. Syed Muhammad ad AF, Awad A, Saidur R et al (2018) Recent advances in cleaner hydrogen productions via thermo-catalytic decomposition of methane: admixture with hydrocarbon. Int J Hydrog Energy. https://doi.org/10.1016/j.ijhydene.2018.08.091
4. Zhou L, Enakonda LR, Li S et al (2018) Iron ore catalysts for methane decomposition to make CO_x free hydrogen and carbon nano material. J Taiwan Inst Chem Eng 87:54–63. https://doi.org/10.1016/j.jtice.2018.03.008
5. Zhou L, Harb M, Hedhili MN et al (2017) Microemulsion prepared $Ni_{88}Pt_{12}$ for methane cracking. RSC Adv 7:4078–4082. https://doi.org/10.1039/C6RA25069F
6. Zhou L, Enakonda LR, Saih Y et al (2016) Catalytic methane decomposition over Fe-Al_2O_3. Chemsuschem 9:1243–1248. https://doi.org/10.1002/cssc.201600310
7. Zhou L, Basset JM (2016) Unsupported NiPt alloy metal catalysts prepared by water-in-oil (W/O) microemulsion method for methane cracking. Fuel 181:805–810. https://doi.org/10.1016/j.fuel.2016.05.067
8. Reshetenko TV, Avdeeva LB, Ushakov VA et al (2004) Coprecipitated iron-containing catalysts (Fe-Al_2O_3, Fe-Co-Al_2O_3, Fe-Ni-Al_2O_3) for methane decomposition at moderate temperatures: part II. Evolution of the catalysts in reaction. Appl Catal A 270:87–99. https://doi.org/10.1016/j.apcata.2004.04.026
9. C Deniz, N Karatepe (2013) Hydrogen and carbon nanotube production via catalytic decomposition of methane. In: Proceedings of the Carbon Nanotubes, Graphene, and Associated Devices, vol 8814, SPIE. https://doi.org/10.1117/12.2023968
10. Torres D, De Llobet S, Pinilla JL et al (2012) Hydrogen production by catalytic decomposition of methane using a Fe-based catalyst in a fluidized bed reactor. J Nat Gas Chem 21:367–373. https://doi.org/10.1016/S1003-9953(11)60378-2
11. Li Y, Zhang B, Xie X et al (2006) Novel Ni catalysts for methane decomposition to hydrogen and carbon nanofibers. J Catal 238:412–424. https://doi.org/10.1016/j.jcat.2005.12.027
12. Takenaka S, Kobayashi S, Ogihara H, Otsuka K (2003) Ni/SiO_2catalyst effective for methane decomposition into hydrogen and carbon nanofiber. J Catal 217:79–87. https://doi.org/10.1016/S0021-9517(02)00185-9
13. Wang G, Jin Y, Liu G, Li Y (2013) Production of hydrogen and nanocarbon from catalytic decomposition of methane over a Ni-Fe/Al_2O_3 catalyst. Energy Fuels 27:4448–4456. https://doi.org/10.1021/ef3019707
14. Dunker AM, Kumar S, Mulawa PA (2006) Production of hydrogen by thermal decomposition of methane in a fluidized-bed reactor—effects of catalyst, temperature, and residence time. Int J Hydrog Energy 31:473–484. https://doi.org/10.1016/j.ijhydene.2005.04.023
15. Muradov N (2001) Catalysis of methane decomposition over elemental carbon. Catal Commun 2:89–94. https://doi.org/10.1016/S1566-7367(01)00013-9
16. Urdiana G, Valdez R, Lastra G et al (2018) Production of hydrogen and carbon nanomaterials using transition metal catalysts through methane decomposition. Mater Lett 217:9–12. https://doi.org/10.1016/j.matlet.2018.01.033
17. Christian B, Lødeng R, Holmen A (2008) A review of catalytic partial oxidation of methane to synthesis gas with emphasis on reaction mechanisms over transition metal catalysts. Appl Catal A 346:1–27. https://doi.org/10.1016/j.apcata.2008.05.018
18. Zhang L, Aboagye A, Kelkar A (2014) A review: carbon nanofibers from electrospun polyacrylonitrile and their applications. J Mater Sci 49:463–480. https://doi.org/10.1007/s10853-013-7705-y
19. Inagaki M, Yang Y, Kang F (2012) Carbon nanofibers prepared via electrospinning. Adv Mater 24:2547–2566. https://doi.org/10.1002/adma.201104940
20. Garg K, Bowlin GL, Garg K, Bowlin GL (2014) Electrospinning jets and nanofibrous structures. Biomicrofluidics 5:013403. https://doi.org/10.1063/1.3567097
21. Liu W, Zhang H, Li D et al (2013) Study on needle and needleless electrospinning for nanofibers. Adv Mater Res 752:276–279. https://doi.org/10.4028/www.scientific.net/AMR.750-752.276
22. Jirsak O, Petrik S (2015) Recent advances in nanofibre technology: needleless electrospinning. Int J Nanotechnol 9:8–9. https://doi.org/10.1504/IJNT.2012.046756
23. Streckova M, Orinakova R, Mudra E et al (2018) Design of electroactive carbon fibers decorated with metal and metal-phosphide nanoparticles for hydrogen evolution technology. Energy Technol 6:1310–1331. https://doi.org/10.1002/ente.201700879
24. Tang Yufeng, Huang Fugiang, Zhao Wei, Liu Zhangiang, Wan Dongyun (2012) Synthesis of graphene-supported $Li_4Ti_5O_{12}$ nanosheets for high rate battery application. J Mater Chem 22:11257–11260. https://doi.org/10.1039/c2jm30624g
25. Wang L, Lachawiec AJ, Yang RT (2013) Nanostructured adsorbents for hydrogen storage at ambient temperature: high-pressure measurements and factors in fluencing hydrogen spillover. RSC Adv 3:23935–23952. https://doi.org/10.1039/c3ra44216k
26. Syed Muhammad ad AF, Awad A, Saidur R et al (2018) Recent advances in cleaner hydrogen productions via thermo-catalytic decomposition of methane: admixture with hydrocarbon. Int J Hydrog Energy 43:18713–18734. https://doi.org/10.1016/j.ijhydene.2018.08.091
27. Suelves I, Pinilla JL, Lázaro MJ et al (2009) Effects of reaction conditions on hydrogen production and carbon nanofiber properties generated by methane decomposition in a fixed bed reactor using a NiCuAl catalyst. J Power Sour 192:35–42. https://doi.org/10.1016/j.jpowsour.2008.11.096
28. Muradov N, Smith F, T-Raissi A (2005) Catalytic activity of carbons for methane decomposition reaction. Catal Today 102–103:225–233. https://doi.org/10.1016/j.cattod.2005.02.018
29. Dufour A, Celzard A, Ouartassi B et al (2009) Effect of micropores diffusion on kinetics of CH_4 decomposition over a wood-derived carbon catalyst. Appl Catal A 360:120–125. https://doi.org/10.1016/j.apcata.2009.02.033
30. Demicheli MC, Ponzi EN, Ferretti OA, Yeramian AA (1991) Kinetics of carbon formation from CH_4-H_2mixtures on nickel-alumina catalyst. Chem Eng J 46:129–136. https://doi.org/10.1016/0300-9467(91)87004-T
31. Kuvshinov GG, Mogilnykh YI, Kuvshinov DG (1998) Kinetics of carbon formation from CH_4-H_2mixtures over a nickel containing catalyst. Catal Today 42:357–360. https://doi.org/10.1016/S0920-5861(98)00115-1
32. Borghei M, Karimzadeh R, Rashidi A, Izadi N (2010) Kinetics of methane decomposition to COx-free hydrogen and carbon nanofiber over Ni-Cu/MgO catalyst. Int J Hydrog Energy 35:9479–9488. https://doi.org/10.1016/j.ijhydene.2010.05.072
33. Moliner R, Suelves I, Lázaro MJ, Moreno O (2005) Thermocatalytic decomposition of methane over activated carbons: influence of textural properties and surface chemistry. Int J Hydrog Energy 30:293–300. https://doi.org/10.1016/j.ijhydene.2004.03.035
34. Presland AEB, Walker PL Jr (1969) Growth of single-crystal graphite by pyrolysis of acetylene. Carbon 7:1–4. https://doi.org/10.1016/0008-6223(69)90002-5
35. Baird T, Fryer JR, Grant B (1974) Carbon formation on iron and nickel foils by hydrocarbon pyrolysis- reactions at 700°C. Carbon 12:591–602. https://doi.org/10.1016/0008-6223(74)90060-8
36. Li Y, Li D, Wang G (2011) Methane decomposition to COx -free hydrogen and nano-carbon material on group 8–10 base

metal catalysts: a review. Catal Today 162:1–48. https://doi.org/10.1016/j.cattod.2010.12.042
37. Konieczny A, Mondal K, Wiltowski T, Dydo P (2008) Catalyst development for thermocatalytic decomposition of methane to hydrogen. Int J Hydrog Energy 33:264–272. https://doi.org/10.1016/j.ijhydene.2007.07.054

Affiliations

K. Sisáková[1] · A. Oriňak[1] · R. Oriňaková[1] · M. Strečková[2] · J. Patera[3] · A. Welle[4] · Z. Kostecká[5] · V. Girman[6]

[1] Department of Physical Chemistry, Chemistry Institute, Faculty of Science, P. J. Šafárik University in Košice, Moyzesova 11, 041 54 Košice, Slovakia

[2] Institute of Materials Research, Slovak Academy of Science, Watsonova 47, 040 01 Kosice, Slovakia

[3] Department of Organic Technology, University of Chemistry and Technology Prague, Technická 5, Praha 6 – Dejvice, 16628 Prague, Czech Republic

[4] Karlsruhe Institute of Technology (KIT), Institute of Functional Interfaces (IFG) and Karlsruhe Nano Micro Facility (KNMF), Hermann-von-Helmholtz-Platz 1, 76344 Eggenstein-Leopoldshafen, Germany

[5] Department of Chemistry, Biochemistry and Biophysics, University of Veterinary Medicine and Pharmacy, Komenského 68/73, 041 81 Kosice, Slovakia

[6] Institute of Physics, Faculty of Science, P. J. Šafárik University, Park Angelinum 9, 040 01 Kosice, Slovakia